Computer Physics Communications 297 (2024) 109038

Contents lists available at ScienceDirect

Computer Physics Communications

journal homepage: www.elsevier.com/locate/cpc

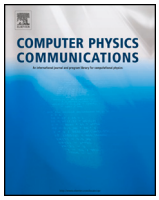

Computer Programs in Physics

Tiresia: A code for molecular electronic continuum states and photoionization ☆,☆☆

Daniele Toffoli [a], Sonia Coriani [b,c], Mauro Stener [a], Piero Decleva [a,d,*]

[a] Dipartimento di Scienze Chimiche e Farmaceutiche, Università degli Studi di Trieste, Via L. Giorgieri 1, I-34127 Trieste, Italy
[b] DTU Chemistry, Technical University of Denmark, Kemitorvet Building 207, DK-2800 Kongens Lyngby, Denmark
[c] Department of Chemistry, Norwegian University of Science and Technology, NTNU, N-7491 Trondheim, Norway
[d] Istituto Officina dei Materiali, IOM-CNR, c/o Area Science Park Basovizza, S.S. 14 – Km. 163,5 I-34149 Trieste, Italy

ARTICLE INFO

Keywords:
B-spline basis
Electronic continuum
Molecular photoionization
Electronic wavepackets

ABSTRACT

The `Tiresia` program [1] provides access to numerically accurate solutions of the one-particle Schrödinger equation for highly excited states of complex polyatomic molecules, both bound and continuum, that cannot be described by conventional Quantum Chemistry approaches. It is based on an expansion of the required solution in a local multicentric basis set, with primitive functions built as products of a radial B-spline times a real spherical harmonic. In conjunction with Density Functional Theory (DFT), it has been extensively employed in a large variety of photoionization studies, also for rather large systems. Highly excited bound states as well as wavepacket propagation can also be accurately described. In fact, the flexibility of the basis essentially allows accurate solutions of linear operator equations, like Poisson or inhomogeneous perturbative equations, which are employed in the code. The program is parallelized with standard MPI-I instructions and makes extensive use of the `Scalapack` linear algebra library. Ancillary programs are available for the evaluation of photoionization cross sections and angular distributions from randomly to fully oriented molecules.

Program summary

Program Title: Tiresia
CPC Library link to program files: https://doi.org/10.17632/fcrjxwgjxh.1
Licensing provisions: GPLv3
Programming language: Fortran77, Fortran90, MPI
Supplementary material: Program manual document
Nature of problem: Accurate solutions for highly excited and continuum electronic states in complex polyatomic molecules. Molecular photoionization cross sections and angular distributions under high energy, high-intensity radiation pulses from Synchrotron radiation and laser sources, photoelectron imaging in pump-probe experiments, basis for electronic wavepackets under ultrafast or nonperturbative excitation.
Solution method: Solution of the Schrödinger and similar linear operator equations in a finite domain is obtained via basis set expansion. Flexible basis set, that may approach practical completeness within the domain, is obtained as a multicenter set of B-spline radial functions times spherical harmonics. Accurate numerical integration is employed for the evaluation of matrix elements, and conventional diagonalization for bound states, or Galerkin approach for the full multichannel solution in the continuum. Full hamiltonian and dipole matrices in the spectral basis are available for time propagation. DFT many-body description is available, and strong correlations in the bound states may be incorporated via Dyson orbitals.
Additional comments including restrictions and unusual features: The code is noted for computational efficiency, which allows fast yet reasonably accurate photoionization calculations for medium-sized molecules, allowing,

☆ The review of this paper was arranged by Prof. Jimena Gorfinkiel.
☆☆ This paper and its associated computer program are available via the Computer Physics Communications homepage on ScienceDirect (http://www.sciencedirect.com/science/journal/00104655).

* Corresponding author at: Dipartimento di Scienze Chimiche e Farmaceutiche, Università degli Studi di Trieste, Via L. Giorgieri 1, I-34127 Trieste, Italy.
E-mail addresses: toffoli@units.it (D. Toffoli), soco@kemi.dtu.dk (S. Coriani), stener@units.it (M. Stener), decleva@units.it (P. Decleva).

https://doi.org/10.1016/j.cpc.2023.109038
Received 13 June 2023; Received in revised form 18 October 2023; Accepted 27 November 2023
Available online 6 December 2023
0010-4655/© 2023 The Author(s). Published by Elsevier B.V. This is an open access article under the CC BY license (http://creativecommons.org/licenses/by/4.0/).

e.g., calculations at many molecular geometries as required to describe time-resolved photoelectron spectra in pump-probe experiments.

1. Introduction

Many chemical processes involve only the electronic ground state, or excited states confined to the manifold of valence orbitals, i.e. orbitals, both occupied and virtual, that are physically well described within the space spanned by the set of low-lying atomic orbitals of the constituent atoms, the so called LCAO basis. These are the domain of Quantum Chemistry (QC) [2,3], which has developed an impressive array of methods and programs for their description and to attack the difficult correlation problem, or many-body effects. At the core of the description are basis sets of Gaussian Type Orbitals (GTO), or more rarely Slater Type Orbitals (STO), that can be augmented to describe polarization and correlation effects.

However, it is difficult for these approaches to describe situations where electrons are forced by external perturbations to depart significantly from the valence manifold, giving states of highly oscillatory nature. This is the case of photoionization, not only a landmark in the development of Quantum Mechanics since Einstein's interpretation of the photoelectric effect, but actually a very common phenomenon, which is the dominant interaction of matter with radiation from VUV till very high energies. In fact, for the majority of molecules, the bulk of oscillator strength in photoabsorption lies in the photoionization region [4]. More broadly, the development of radiation sources, lasers and Synchrotrons, and more recently free electron lasers (FELs), and the concurrent advances in electron detectors, are providing some of the most sophisticated tools for the study of molecular structure and dynamics, both nuclear and electronic, in the ultrafast domain [5]. Short electromagnetic pulses excite nonstationary states whose evolution is followed in time, mostly through the use of a second, analyzing pulse (pump-probe experiments), for which photoionization is one of the main probes. More details are provided by angular distributions of photoelectrons, which can also probe molecular chirality, from single photon to more elaborate ionization experiments. Actually, coincidence techniques in electron/ion detection, and alignment procedures via laser pumping provide an additional wealth of angular distribution parameters that afford a much richer information on molecular states, up to the so-called complete experiment, in which a full set of dipole transition matrix elements, including relative phases, can be experimentally obtained [6]. More recently, even energy derivatives of the phases, associated with Wigner time delays, can be addressed by several techniques and are actively investigated [7].

It is to this scientific area that the `Tiresia` program [1] is geared to. Several approaches have already been developed for molecular photoionization although becoming generally available quite recently, e.g., the `ePolyScat` [8,9] and the `UKRmol+` R-Matrix code [10], to quote only the most widespread, or the `XCHEM` [11,12] that is currently released. At variance with these approaches, originally aimed at the accurate description of small systems, `Tiresia` was designed at the outset with complex polyatomic molecules in mind. That has demanded some compromise with the description of multielectron effects, for which a density functional theory (DFT) approach appeared as a computationally effective method, that has proved to give a good description of the experimental observables at a rather modest computational cost. An effective way to generalize to an accurate description of correlation effects in the bound states, notably to allow photoionization from open-shell systems and excited states, or to multielectron excitations in the final states, is the coupling of DFT continua to Dyson orbitals [13–17] relative to the initial/final bound states couple, which can be accurately computed by QC approaches and are now available in several QC codes, see e.g. Refs. [18–20].

The core problem of approaches aiming to describe the electronic continuum is an accurate and efficient algorithm for the solution of the one-particle Schrödinger equation

$$h\varphi = E\varphi \tag{1}$$

for both the bound ($E < 0$) and continuum ($E > 0$) eigenstates. Here,

$$h = -\frac{1}{2}\Delta + V \tag{2}$$

where V is a one-particle operator, often a local potential function of the electron coordinates $V(\mathbf{r})$, or in general non local, like the exchange operator in Hartree-Fock (HF). In the atomic case, due to spherical symmetry, it is natural to utilize one-dimensional radial grids together with analytical angular functions (Spherical Harmonics) and employ finite difference approaches for the radial coordinate. The same approach (Single Center, or One Center expansion, OCE) can also be useful in molecules and has been widely employed [8,21,22]. It has the merit of a natural representation of the wave function in the asymptotic region, and in general far from the molecular core. However, the loss of spherical symmetry couples different partial waves, and moreover Coulomb cusps far from the expansion center are poorly represented by a partial wave expansion, that converges very slowly in the case of heavy atoms far from the expansion center. The same problem also plagues full three-dimensional grids, generally in Cartesian coordinates, which additionally do not give a natural representation of the outer region, while it proves difficult to generate and exploit adaptive grids tailored to the molecular potential. In fact, the best solution is indicated by the spectacular success of the LCAO approach in molecules, with spherical basis functions distributed over all nuclei. Indeed, they generate a smooth transition from an almost spherical environment close to one nucleus to the analogous environment close to a different one. Therefore, an optimal choice appears to be the use of a multicentric basis set, comprising a long-range OCE part with special bases designed to describe the oscillatory behavior and reach the asymptotic limit, and a limited number of additional sets on each atom to take care of the Coulomb cusp [23,24]. The latter sets may be standard or specially designed GTOs or STOs, or additional special functions. Different combinations are chosen in recent codes [10,11]. For brevity, we shall refer to a multicentric basis as LCAO in the following.

Operators are then represented as matrices on the basis, and bound eigenstates may be obtained by conventional diagonalization. In the case where actual continuum eigenvectors are needed, specialized algorithms are required to obtain the full set of linearly independent degenerate eigenvectors. Several variants are in use, like the R-matrix approach [25], the imposition of specific boundary conditions [11], the Galerkin approach [26–28]. If the basis is accurate, all these approaches will give essentially the same result, although the computational efficiency may vary.

The one-electron hamiltonian may be used as approximate description of the system, like in the static HF or the equivalent DFT formulation, or can be employed in more elaborate descriptions of the many-body problem, like RPA [29] or TDDFT [30,31], or in configuration interaction formulations, like the well known Close-Coupling approach [25]. Transition dipole matrix elements between bound and continuum states allow the calculation of fully differential photoionization cross sections, from randomly oriented molecules to various degrees of alignment orientation, till the full Molecular Frame Photoelectron Angular Distributions (MFPADS). A numerically accurate "complete" basis may also be exploited for the solution of the time-dependent Schrödinger equation (TDSE), either in the primitive basis, or in the spectral basis obtained from a full diagonalization of the hamil-

tonian, which offers different advantages. Moreover, the ability to fully describe eigenstates of the system allows analysis of the composition of the final wavepacket, and again the fully differential transition properties. A complete basis can also afford accurate treatment of perturbative formulations, like the Lowest Order Perturbation Theory description of multiphoton transitions (LOPT).

We shall now describe the specific features and capabilities of the `Tiresia` code based on the DFT hamiltonian.

2. The static DFT approach

The DFT formalism [32] describes the ground state (GS) of a molecule through the electron density ρ. In practice, the Kohn-Sham (KS) approach builds the density as given by one determinant of occupied orbitals:

$$\Phi_0 = |\phi_1 \phi_2 \dots \phi_N\rangle, \quad \rho = \sum_i |\phi_i|^2, \tag{3}$$

which are the solutions of the KS hamiltonian

$$h_{\rm KS}\phi_i = E_i\phi_i \ , \tag{4}$$

with $h_{\rm KS}$ defined as usual:

$$h_{\rm KS} = -\frac{1}{2}\Delta + V_{\rm en} + V_{\rm C}(\rho) + V_{\rm XC}(\rho) \ . \tag{5}$$

In Eq. (5), the first term represents the kinetic energy operator, the second the nuclear attraction, the third the classical Coulomb potential associated with the density ρ, and the fourth is the exchange-correlation potential, a functional of the density, an unknown quantity for which various approximate forms have been developed. In the simplest approximation, it is a local function of the density, i.e., $V_{\rm XC}(\mathbf{r}) = V_{\rm XC}(\rho(\mathbf{r}))$. The equations are very similar to the HF ones, differing only in the substitution of the ab-initio exchange term, which is non local and depends on the full density matrix, with the $V_{\rm XC}$ potential, which only depends on ρ. Still, the DFT form succeeds in eliminating some pathologies of HF, and in including some correlation in an average way, giving results either similar to or often improved over the HF ones.

The solution of the GS DFT equations requires a self-consistent procedure, as in the HF case. Once the appropriate density is obtained, it defines a "static" KS (or DFT) hamiltonian (eq. (4)) that can be diagonalized to extract excited state eigenvectors, both bound and continuum; N-particle excited states are obtained by substituting one (or more) occupied orbitals with a virtual one, giving, i.e., singly excited states

$$\Phi_i^a = |\phi_1 \dots \phi_{i-1}\phi_a\phi_{i+1} \dots \phi_N\rangle = a_a^\dagger a_i \Phi_0 \ , \tag{6}$$

and so on, described as single determinants. A complete set of N-particle states are obtained in this way, as eigenstates of a mean-field hamiltonian $H_0 = h(1) + \cdots h(N)$, which could also be used in evaluating perturbation theory (PT) formulas, or in the solution of the TDSE. Dipole matrix elements reduce to single particle matrix elements between an initial orbital ϕ_i and a final orbital ϕ_a (bound or continuum).

Three choices of local $V_{\rm XC}$ potentials are available in the code: the old Slater's X_α potential [33], which is still in use [34], the standard LDA VWN potential [35], and the LB94 potential [36]. The latter was developed to improve the description of polarizabilities, and therefore excited states, and it has a correct asymptotic behavior producing a Coulomb tail at large distances, at variance with the former ones that decay exponentially for a neutral system. Actually, better results with X_α or VWN are obtained using the so-called transition state potential [33,37] which corresponds to a density with half an electron removed from the ionized orbital. Another possibility is the enforcement of a pure Coulomb tail, from a preset radius onward, or when the density falls below a prefixed threshold. This procedure becomes necessary if very long OCE expansions, in the range of several hundreds of au or larger, are needed, since the evaluation of the $V_{\rm XC}$ potential becomes numerically unstable.

An advantage of the LB94 potential is that, in practice, the GS potential proves an optimal choice for the description of all ionized states, so that one single calculation provides results for the cross sections of all primary ionic states, from the outer valence to the deep core states. The specific functional form of the LB94 potential is, however, tied to the assumption of an exponentially decaying density. Numerically, this is well satisfied by the use of STO basis functions in the initial density calculation, as is implemented in the ADF DFT code [38,39], while the use of GTO bases often gives long-range oscillations which can produce some unphysical results in the cross sections. `Tiresia` was historically developed based on ADF densities, and an interface to this code is provided. With GTO bases, it may be better to revert to X_α or VWN that are more stable. Examples are provided.

The pure DFT approach gives as a general rule a good description of ionization of single-hole (primary) ionic states. In the case of more complex ionization processes, such as ionization from open shell or excited states, or multielectron excitations in the final states (satellites), and in general in the case of strong correlation effects in the initial or final bound states, the DFT approach can be easily generalized by the use of Dyson orbitals [13,14,16]. A Dyson orbital pertains to a couple of bound states, an initial N-particle Ψ_0^N and a final $(N-1)$ particle Ψ_I^{N-1}. It is defined as

$$\varphi_{I0}^D(1) = \sqrt{N}\int \Psi_I^*(2,\dots,N)\Psi_0(1,2,\dots,N)dx_2 \dots dx_N \tag{7}$$

and can be computed with highly correlated ab initio wavefunctions. Generalizing the scattering formalism to a single channel approach, with the final state expressed as an antisymmetrized product of a bound ionic state and a continuum orbital, $\Psi_{IEj}^N = \mathcal{A}\Psi_I^{N-1}\phi_{Ej}$, the many-particle dipole matrix element reduces to a single-particle one involving the continuum and Dyson orbitals, plus a conjugate contribution which is generally small and neglected [15,40,17]

$$D_{IEj,k} = \langle \Psi_I \phi_{Ej}|D_k|\Psi_0\rangle \simeq \langle \phi_{Ej}|d_k|\varphi_{I0}^D\rangle \tag{8}$$

In `Tiresia`, Dyson orbitals computed with ab initio QC codes (for instance, `OpenMolcas` [41], `Q-Chem` [42] and e^T [43]) can be read and used as initial states for the calculation of dipole amplitudes, with minimal modifications.

3. The basis

The primitive basis functions employed in `Tiresia` are products of a radial B-spline function times a real spherical harmonics:

$$\chi_{ilm} = \frac{1}{r}B_i(r)Y_{lm}^R(\theta,\phi) \ . \tag{9}$$

These are used both for the OCE expansion and for the LCAO ones, the latter centered on the atomic sites.

B-spline functions are well documented [44,24]. We recall here simply that they are defined over a given interval, $[0, R]$ in our case, divided into subintervals by a non-decreasing sequence of points, called *knots*. They are made of polynomial pieces of a fixed order k (degree $k-1$), one over each subinterval, spanning $(k+1)$ consecutive knots and identically zero outside, joined with chosen continuity across adjacent subintervals. They have been designed to approximate arbitrarily well any smooth function over the interval by suitably choosing the set of knots, i.e., the stepsize of the grid. In this sense, they constitute a complete set and usually converge extremely fast. In practice, given the order and the interval, the basis is completely defined by the set of knots. For our purpose, it is customary to place k knots at the endpoints, and single knots inside. This gives a full set of B-splines over the interval, of maximum continuity at the inner knots. At each end, the first and the last spline are nonzero. To satisfy the boundary condition at the origin, the first spline is deleted. This gives, in total, $k+n-2$

functions in the case of n subintervals. For bound states also the last spline is deleted, ensuring zero at the outer boundary, while it is kept for the description of the continuum states, which are generally nonzero at the outer boundary. The accuracy of the basis increases sharply with k, with a negligible increase on the typical size of the basis. However, numerical errors limit the maximum value of k that can be employed. Our standard choice is $k = 10$, the maximum that proved viable [28]. A long range $[0, R_{max0}]$ is employed for the OCE expansion, while short ranges $[0, R_{maxp}]$ are employed for the LCAO expansions. For the latter, actually, some of the last splines (default $m = 3$) are deleted, ensuring continuity of the wave function up to the second derivative over the whole space. In fact, the range of the LCAO expansions is restricted to be non overlapping, but this is in practice no limitation, and often shorter ranges are employed, as discussed later.

The sequence of knots can be read as input, but the most common is a linear grid. The continuum wavefunction is roughly a plane wave, oscillating regularly with a wavelength associated to the electron momentum k, $E = k^2/2$, $\lambda = 2\pi/k$. It is thus natural to choose a constant step size, of the order of $h = 1/k_{max}$, related to the maximum electron momentum (energy) that one needs to describe. The range of the expansion is determined by the requirement that all bound states of interest, as well as the density, are negligible outside it. At this point the potential is of pure multipolar form, and, for photoionization, is dominated by the pure Coulomb term. The neglect of dipolar and higher terms when fitting to pure Coulomb asymptotic behavior can be checked by repeating calculations with increasing R_{max0}. Normally, also for polar molecules, results for cross sections and angular distributions are generally stable, at the level of one percent or better, after a few tens of atomic units. Fig. 1 illustrates this for three valence and one core ionization of H_2O, computed with origin on Oxygen, $R_{max0} = 25.$ and 100. au, and Oxygen further displaced on the z axis by 1.0 au, $R_{max0} = 25.$ au.

More delicate observables, like individual phase shifts for time delay evaluation, may require somewhat longer ranges. The role of multipolar components may become very important in photodetachment, or electron scattering, especially at low kinetic energies. While it is not problematic to employ very large R_{max0}, the use of a fitting routine including the lowest multipoles may be a more efficient alternative. For photoionization, a typical range of around 20-30 au is in general adequate, with the total number of B-splines in the order of hundred. For special purposes, either very diffuse states or wavepacket propagation, larger ranges in the hundreds or thousands of au may be employed, without loss of precision or numerical stability. For bound states a natural grid is exponential, and in fact, with this choice, very high Rydberg states can be described. However, the same grid is employed for both bound and continuum states in photoionization to ease the computation of the dipole matrix elements, so the linear grid is the common choice. In summary, both linear and exponential grids for the OCE expansion are internally provided, by specifying (in input) the outer radius R_{max0} and the number of steps (or stepsize). For the short LCAO expansions, a linear grid is always used, with similar step sizes as for the OCE. In both cases, some additional knots may be required, as explained below.

As angular functions, real spherical harmonics are employed. Our definition is

$$Y_{lm}^R = \left\{ \frac{1}{\sqrt{2\pi}} P_l(\cos\theta),\ \frac{1}{\sqrt{\pi}} P_l^{|m|}(\cos\theta)\cos|m|\phi,\ \frac{1}{\sqrt{\pi}} P_l^{|m|}(\cos\theta)\sin|m|\phi \right\} \tag{10}$$

for $m = 0, m > 0, m < 0$, respectively. For each basis, the full set of Y_{lm}^R are employed up to a maximum value L_{max}. For the LCAO basis, L_{maxp} is very low, typically 1 or 2 for light atoms, while L_{max0} for the OCE is generally much larger, up to several tens. This is because of the need to describe the short-range anisotropy of the wave function outside the LCAO expansions, as well as to describe all partial waves that are populated in the continuum. The latter increases fast with increasing electron momentum.

From all of the above, it follows that the dimension of the basis is in general fully dominated by the dimension of the OCE expansion, while the LCAO part has only a modest impact on the total dimension. It proves nonetheless very important to ensure fast convergence of the basis and to describe deep core states. A couple of examples will be given later.

The program makes full use of point group symmetry, including the nonabelian ones. To this purpose, the primitive basis is fully symmetry adapted [45–47]. For the OCE:

$$\chi_{ij\lambda\mu} = \frac{1}{r} B_i(r) X_{j\lambda\mu}(\theta,\phi) \quad X_{j\lambda\mu}(\theta,\phi) = \sum_m b_{mj\lambda\mu} Y_{lm}^R(\theta,\phi) \quad l = l(j), \tag{11}$$

where $(\lambda\mu)$ are labels for the irreducible representation and the degenerate subspecies, and j counts the linearly independent combinations of the $(2l+1)$ spherical harmonics within the same irrep. For the LCAO part, the linear combination is extended to all atoms which are symmetry equivalent

$$\chi_{pij\lambda\mu} = \sum_{q\in p} \frac{1}{r_q} B_i(r_q) \sum_m b_{qmj\lambda\mu} Y_{lm}^R(\theta_q,\phi_q) \quad l = l(j) \tag{12}$$

where the index p runs over the sets of inequivalent atoms, and q over the equivalent atoms in set p. Expansion coefficients b are obtained by application of the usual projection and shift operators of point group theory to the primitive basis. The final basis is

$$\{\chi_{ij\lambda\mu}\} \cup \{\chi_{1ij\lambda\mu}\} \cup \cdots \cup \{\chi_{rij\lambda\mu}\} \tag{13}$$

where the first is the OCE basis followed by the LCAO bases, one for each of the r inequivalent sets of atoms.

An important issue is the numerical linear independence of the basis, which is vital for the numerical stability of the algorithms. The OCE basis, independently of its size, is always well conditioned, because of the limited overlap of the B-spline functions and the orthonormality of the spherical harmonics. Adding LCAO functions strongly worsens the situation, as it can become in principle overcomplete. This is signaled by a strong decrease of the smallest eigenvalues of the overlap (S) matrix. It is for this reason that the range of the LCAO functions has to be severely limited. The problem is most severe for centers close to the origin, but eases for more distant centers, precisely where larger ranges are more important. It also worsens with increasing L_{max0} of the OCE expansion, which then requires shorter LCAO ranges. This problem is common to all LCAO approaches and it is often tackled by diagonalizing the S matrix, transforming to the basis of its eigenvectors, and deleting those relative to eigenvalues smaller than a given threshold. We found this procedure not very safe. Instead, the flexibility of a full B-spline basis allows us to control relatively easily the degree of overlap by restricting the LCAO ranges without loss of precision, although it may require some experimentation, monitoring the S matrix eigenvalues in difficult cases.

In summary, the present basis has shown the ability to accurately describe rather large and complex systems, including heavy atoms and deep core states, up to large electron kinetic energies (several keV [48]) with any energy resolution required, and good numerical stability. It may be easily tailored to the specific problem of interest.

4. Evaluation of matrix elements

Extensive numerical integrations are employed. For integrals involving only OCE functions, which are factorized into a radial and an angular part, preliminary partial wave decomposition of integrands is

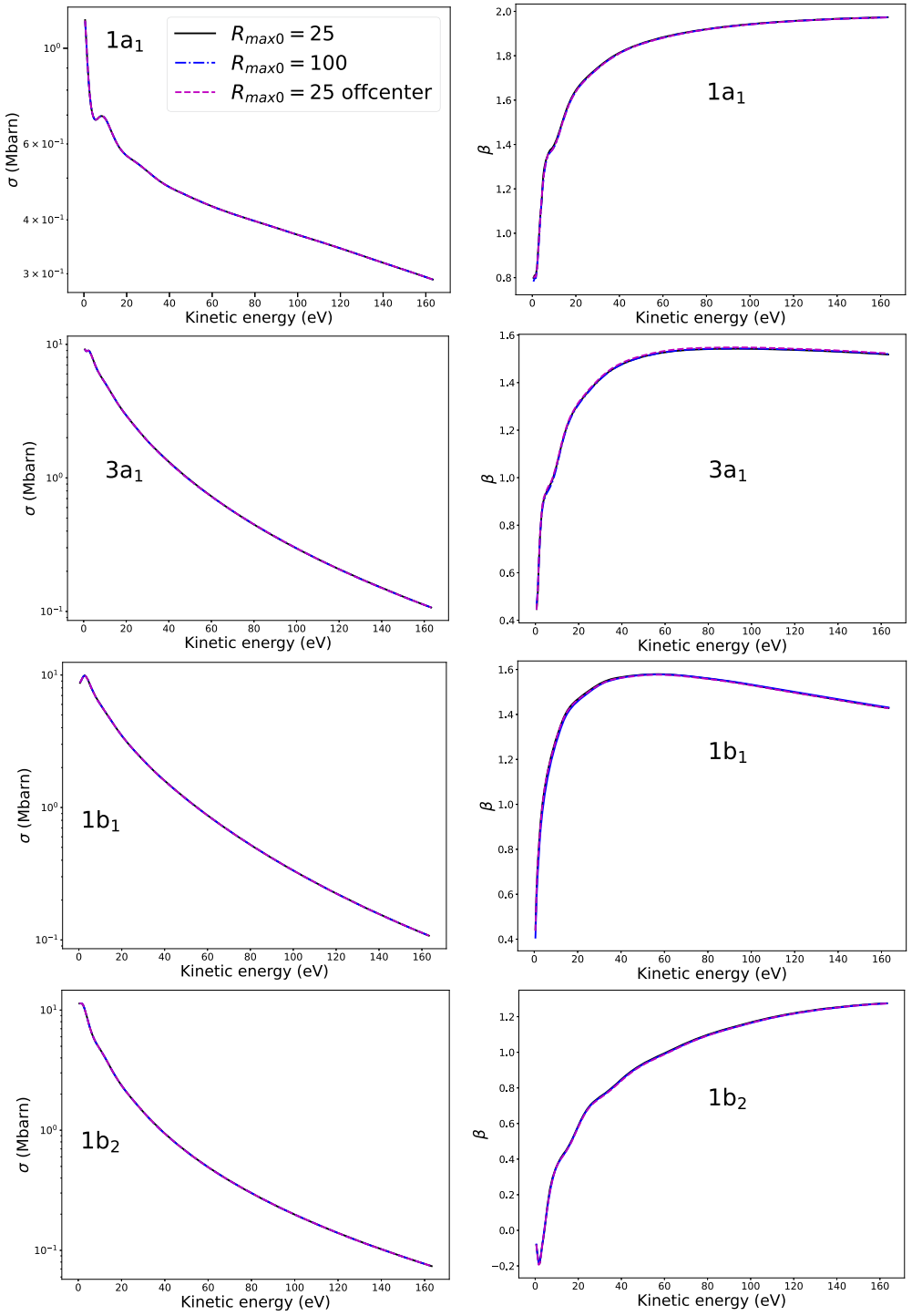

Fig. 1. Convergence of the cross section σ (Mbarn, left panels) and asymmetry parameter β (right panels) of three valence and one core ionization of H_2O computed when varying R_{max0}.

performed. Given an arbitrary function $f(x, y, z)$, one obtains

$$f(r,\theta,\phi) = \sum_{j\lambda\mu} f_{j\lambda\mu}(r) X_{j\lambda\mu}(\theta,\phi) \tag{14}$$

$$f_{j\lambda\mu}(r) = \int X_{j\lambda\mu}(\theta,\phi) f(x,y,z) \sin\theta \, d\theta \, d\phi \tag{15}$$

and

$$\langle \chi_{ij\lambda\mu} | f \rangle = \int B_i(r) f_{j\lambda\mu}(r) r \, dr \tag{16}$$

or

$$\langle \chi_{ij\lambda\mu} | f | \chi_{i'j'\lambda'\mu'} \rangle = \tag{17}$$
$$\sum_{j''\lambda''\mu''} \int B_i(r) f_{j''\lambda''\mu''}(r) B_{i'}(r) \, dr \int X_{j\lambda\mu} X_{j''\lambda''\mu''} X_{j'\lambda'\mu'} \sin\theta \, d\theta \, d\phi$$

where the angular integrals can be expressed in terms of three spherical harmonics, that reduces to a combination of $3j$ symbols.

Radial integrals over B-splines are obtained with high accuracy by Gauss-Legendre (GL) integration over each subinterval, provided that

the integrand is smooth. In case of singularities, as happens with the cusps in the molecular potential due to off center nuclei, to maintain accuracy it is very important that such radial points occur at the endpoints of the subintervals. This is easily accomplished by adding to the original knot sequence additional points corresponding to the radial coordinates of the off-center atoms. In the case of very heavy nuclei, a couple of closely spaced knots around their radial positions may be necessary for the highest accuracy. That is also needed if a heavy atom is present at the origin. The same logic applies to the angular integration over the surface of a sphere, eq (15). Here, the two-dimensional domain $[0,\pi]\times[0,2\pi]$ in (θ,ϕ) variables is integrated by a product of two GL integrations in each dimension. To avoid singularities, however, each angular domain is split into subdomains having as inner points the polar coordinates of the off-center atoms, e.g., $[0,\phi_1],[\phi_1,\phi_2],\dots$ Again, if heavy atoms are present, adding a couple of closely spaced points around its coordinates may be required for high accuracy. This is also the case at the endpoints, like 0 or 2π if an atom lies on such points. Generally, with such choices, very accurate results are obtained. It may be monitored by the value of the numerically integrated electron charge density, which is usually recovered up to 8 or more significant digits. In the case of symmetry, actually, the angular integration range can be restricted to a symmetry unique domain for a totally symmetric integral. The same technique can be employed for non totally symmetric integrands, if a sum over all degenerate subspecies is employed.

The same integration is performed for integrands involving the LCAO functions, in spherical coordinates relative to the corresponding center. Here, no singularities exist in the domain, apart from the origin, and no special points have to be added for the angular domain integration. However, for very high accuracy, each angular domain is linearly divided into a number of subintervals (default is 24). Since the LCAO ranges do not intersect, only two center integrals between an OCE and an LCAO function appear. These are also evaluated in spherical coordinates around the LCAO center. In the case of two-center integrals, the reference systems are rotated so that the new Z axis is from the origin to the LCAO center, and the spherical harmonics are accordingly rotated [23]. This allows to exploit the local cylindrical symmetry, so that ϕ integration becomes analytical. The integrals are then rotated back to the original reference. Moreover, in the case of equivalent centers, integrals are computed only for the first center, the others are obtained by appropriate rotations. Finally, they are combined with the appropriate coefficients to generate the integrals relative to symmetry adapted functions.

It is worth mentioning the evaluation of the matrix elements of the molecular potential. While the nuclear attraction $V_{\rm en}$ and the $V_{\rm XC}$ potentials are simple functions ($V_{\rm en}$ also has an analytic multipolar expansion), the Coulomb part $V_{\rm C}$ requires more work. We exploit the completeness of the basis to obtain $V_{\rm C}$ by solving the Poisson equation in the same basis. By writing the full basis simply as $\{\chi_\nu\}$

$$V=\sum_\nu V_\nu\chi_\nu \quad \rho_\mu=\langle\chi_\mu|\rho\rangle \tag{18}$$

one obtains

$$\sum_\nu \Delta_{\mu\nu}V_\nu=-4\pi\rho_\mu \tag{19}$$

which is a linear inhomogeneous equation that is easily solved for the coefficients V_ν of the potential expansion. The matrix elements $\langle\chi_\mu|V_{\rm C}|\chi_\sigma\rangle$ are evaluated as above from this representation of $V_{\rm C}$. The ability of the basis to accurately represent solutions not only of the operator eigenvalue equation but also of inhomogeneous ones is an important asset, that can be exploited, for instance in PT formulations. Note also the ease of implementation of specific boundary conditions on the solution, by taking appropriate linear combinations of the last basis elements. In the case of $V_{\rm C}$, multipolar boundary conditions, $V'_{lm}/V_{lm}\to-(l+1)/r$, are enforced.

Diagonalization of the bound states, removing the last spline, can be efficiently performed with standard linear algebra (LA) routines (`Scalapack` [49]), up to hamiltonian matrix dimensions up to about 10^5. In the case of continuum states, we note that the full hamiltonian matrix is no longer hermitian, because of the nonzero value of the last spline at the outer boundary. Several algorithms are available to obtain the full set, equal to the number n_o of asymptotic channel functions, of linearly independent continuum eigenvectors. We implemented the Galerkin approach, originally proposed by Froese-Fischer [26,50] in the single channel, and later generalized to the multichannel case [27,28,51]. It aims at the approximate eigenvectors of the matrix $A(E)=H-E\,S$ having minimum eigenvalue (close to zero), i.e., minimizing the residual

$$A(E)c=ac \tag{20}$$

with the smallest a. They can be obtained by inverse iteration starting from an arbitrary guess, iterating the solution of the linear system

$$Ay_i^{k+1}=x_i^k \tag{21}$$

starting from n_o independent (orthonormal) guess vectors, $x_i^0, i=1,n_o$, and reorthonormalizing at each step. We actually found that better performance is obtained employing the product $A(E)^TA(E)$, which moreover is hermitian (symmetric). In practice, one finds that, with a good basis and n_o open channels, the lowest n_o eigenvalues are extremely small and separated from the next by several orders of magnitude, and the inverse iteration usually converges very fast. Occasional instabilities may occur, especially with large calculations involving hundreds of channels, and disappear by slightly changing the energy. In practice this is not an issue, as the cross section is very smooth, and one easily detects an erratic point. Difficult convergence may also occur at very low energies, if the number of channels is "too large", meaning that the high l components have very small amplitude (they do not penetrate the centrifugal barrier) at those energies. Still, cross sections are usually fine, as those high l channels contribute insignificantly. Alternatively, those instabilities disappear by reducing the L_{max0} value.

A grid of continuum energies E_n of interest is selected, and the process is repeated for each of them. As

$$A^TA=H^TH-E(H^TS+S^TH)+E^2S^TS \tag{22}$$

we found convenient to precalculate the three energy-independent product matrices, $H^TH,(H^TS+S^TH),S^TS$ and build A^TA by just summing the three contributions. Then, at each E, an LU decomposition of A^TA is performed, and the inverse iteration is very fast. Since the n_o eigenvectors are degenerate, an arbitrary mixture is obtained at the end of the iteration. To fix them uniquely, one has to fix the asymptotic form, and we chose to normalize them to the K-matrix boundary condition, which has the advantage of keeping the eigenvectors real [46,27]. That is, by fitting the radial parts of the obtained eigenvectors to a linear combination of the regular (f_l) and irregular (g_l) asymptotic solutions close to the outer boundary, the following form of the solutions is obtained

$$\phi_{Ej'\lambda\mu}=\sum_j R_{jj'\lambda}(r)X_{j\lambda\mu} \tag{23}$$

$$R_{jj'\lambda}(r)=f_l(kr)A^\lambda_{jj'}+g_l(k\,r)B^\lambda_{jj'} \tag{24}$$

The two matrices (fitting coefficients) A and B are obtained by equating the values of $R_{jj'\lambda}(r_i)$ to a combination of $f_l(kr_i)$ and $g_l(kr_i)$ at the last two interior knots of the interval. Choosing the last two knots, or the logarithmic derivative at the outer boundary, produces the same result. Then, by transforming

$$\bar R=RA^{-1}\,, \tag{25}$$

the K-matrix form is obtained:

$$\bar{R} \to \delta_{jj'} f_l + K^{\lambda}_{jj'} g_l \quad K = BA^{-1} \quad . \tag{26}$$

It is simple then to transform the resulting eigenvectors, or simply the relative dipole matrix elements, to any other asymptotic form, like the S-matrix

$$S = (1 + iK)(1 - iK)^{-1} \tag{27}$$

or its adjoint $S^{\dagger}$, corresponding to incoming waves $\phi^{(-)}_{Ej\lambda\mu}$ which are the correct form to describe photoionization, and are obtained from the K-matrix normalized solutions by

$$\phi^{(-)} = \phi(1 + iK)^{-1} \quad . \tag{28}$$

The dipole matrix elements

$$D_{Ej\lambda\mu,k,i\lambda'\mu'} = \langle \phi^{(-)}_{Ej\lambda\mu} | d_k | \phi_{i\lambda'\mu'} \rangle \tag{29}$$

can be transformed accordingly. For each energy E_n, the K-matrix (actually, its eigenvalues and eigenvectors) together with the K-normalized dipoles are written on an external file (`fort.20`). They contain all information needed to extract any kind of differential cross section in one-photon ionization, and are processed by additional programs. The dipole matrices are computed for all initial states and continuum channels in all symmetries, and are relatively small. It is useful, in multiphoton PT calculations or wavepacket propagation via numerical solution of the TDSE, to employ the spectral basis obtained by a full diagonalization of the bound hamiltonian, and fully transform the dipole matrix elements to this basis. This is available as a separate facility inside the code. While we do not provide at this time a TDSE propagation algorithm, such approaches have been repeatedly used to study strong field or ultrafast pump-probe processes [52–54]. Also, a facility to analyze a wavepacket at the end of the pulse, by projecting onto continuum states, is available.

The program is parallelized using standard MPI instructions. The computationally intensive parts are numerical integrations and LA operations. Integration requires evaluation and sum of the integrands at a large number of points, that parallelizes trivially, assigning separate groups to each processor, and then collecting the partial sums with an `MPIREDUCE` operation. This parallelizes very efficiently and scales linearly. For LA operations on vectors and matrices parallel `BLAS` and `SCALAPACK` routines [49] are employed. This is a bit more complex, as it requires distributing arrays over processors according to the *block cyclic decomposition* (BCD) [49], which does not map naturally on the block structure of the matrices in the B-spline basis. Some special routines have been devised to transform back and forth between subblocks of the global arrays and local matrices in the BCD structure. Also, LA operations then parallelize quite efficiently, provided that the local blocks are not too small, so that useful parallelism scales up naturally with the size of the problem. Up-to-date tests up to 4K processors have been performed. Typical memory per core needed is about 2GB, larger values may be required in large calculations.

5. Input and program structure

Extensive details are provided in the accompanying manual, as well as illustration of the examples enclosed. For a normal photoionization calculation, most defaults internally provided are generally adequate, and the input is then rather simple.

The minimal input required from the user comprises

- specification of the molecular geometry
- specification of the symmetry group and maximum OCE angular momentum (L_{max0})
- specification of the OCE radial grid (typically R_{max0} and number of subintervals for a linear grid)
- specification of the active symmetries (irreps) and number of occupied orbitals in each symmetry
- specification of the LCAO grid for each nonequivalent atom
- for the continuum, specification of the energy points.

In addition, specification of the angular grid for OCE integration is required, but one can use the defaults provided, which are often quite accurate, and in any case give a good starting point for further refinements, if needed. See the manual for commented examples.

The program is relatively large, with several hundred routines. It can be divided into logically connected blocks, each comprising many routines, generally under control of a driver routine. We may schematize it as follows

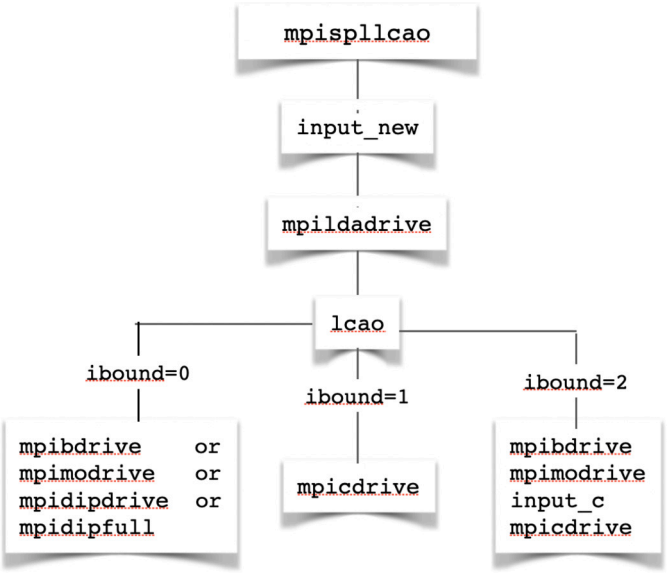

Parameter `ibound=0` directs to a bound state calculation, `ibound=1` to a continuum calculation, `ibound=2` to bound followed by continuum calculation in a single run.

- `mpispllcao` is the main program, initializes and directs the flow
- `input_new` directs all input, read from file 'input'. Reads parameters specifying the flow and several options, performs symmetry analysis, defines the basis, computes array dimensions, and initializes them
- `mpildadrive` computes the molecular potential. Reads the external density, computes the Coulomb potential solving the Poisson equation, and the partial wave decomposition of the full potential for computing OCE matrix elements. Write results on file `fort.23`
- `lcao` computes one- and two-center matrix elements involving LCAO functions, and writes on file `fort.22`. Then symmetrizes the matrix elements.
- `mpibdrive` runs over symmetries, sets up and diagonalize bound state hamiltonian. Writes eigenvectors on external file `fort.11`, or also as parallel MPI file `fort.110`. Computes dipole matrix elements and transitions between bound states for a limited number of eigenvectors.
- `mpimodrive` reads external orbitals from ab initio GTO calculations, from input file `mofile.dat`. These are used to input SCF initial density, or, in the case of Dyson orbitals, are projected onto the B-spline basis, for calculation of transition dipole matrix elements
- `mpidipdrive` transforms dipole matrices to the spectral basis in the case of full diagonalization of the hamiltonian, reads from `fort.11` and `fort.110` and writes results on files `fort.71` and MPI parallel file `dipole.parallel`

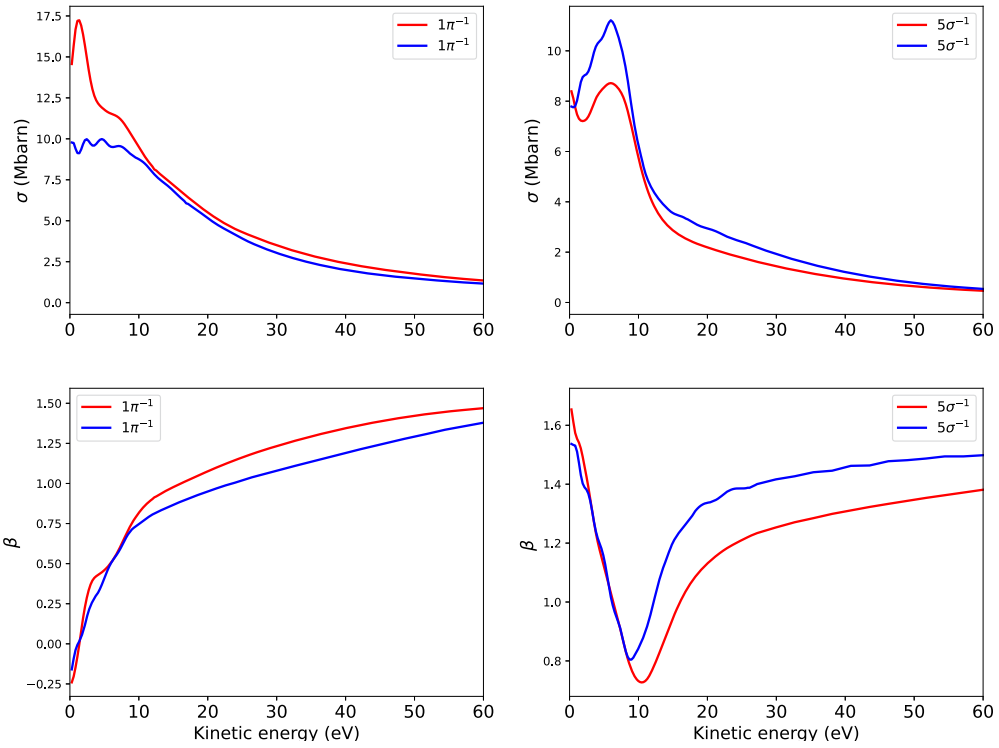

Fig. 2. σ and β parameters relative to photoionization of the 5σ and 1π orbitals of CO. DFT calculations with LB94 potential starting from LB94 density and orbitals in STO functions (red) or HF density and orbitals in GTO (blue). (For interpretation of the colors in the figure(s), the reader is referred to the web version of this article.)

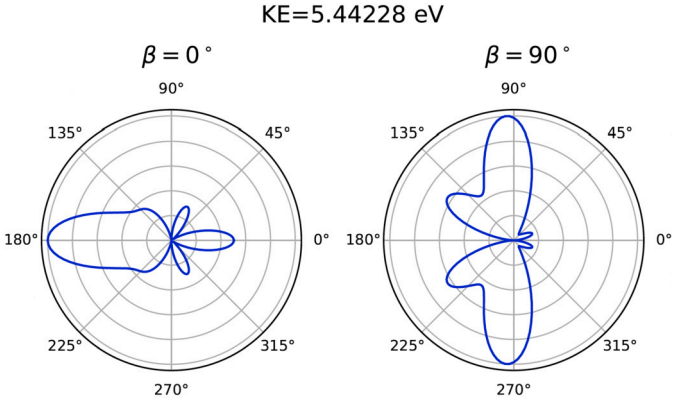

Fig. 3. MFPADS of 5σ of CO, with parallel and perpendicular polarization.

- `mpidipfull` is an old version of calculation of dipole matrices between bound states, less efficient, essentially for checking purpose. Can deal with an intermediate number of vectors. Writes results on file `fort.70`
- `mpicdrive` runs over the symmetries, sets up hamiltonian and overlap matrices for the continuum, runs over the energies and performs inverse iteration to get continuum eigenvectors. Computes dipole transition matrix elements with the initial states from a previous bound state calculation, K-matrix normalized. Writes K-matrices and dipole matrices on file `fort.20`
- `input_c` if `ibound=2`, i.e. bound followed by continuum calculation, after the bound part (`mpibdrive`, `mpimodrive0`) reads a second set of parameters for the continuum calculation, before entering `mpicdrive`.

The typical flow of a calculation with `Tiresia` is illustrated below:

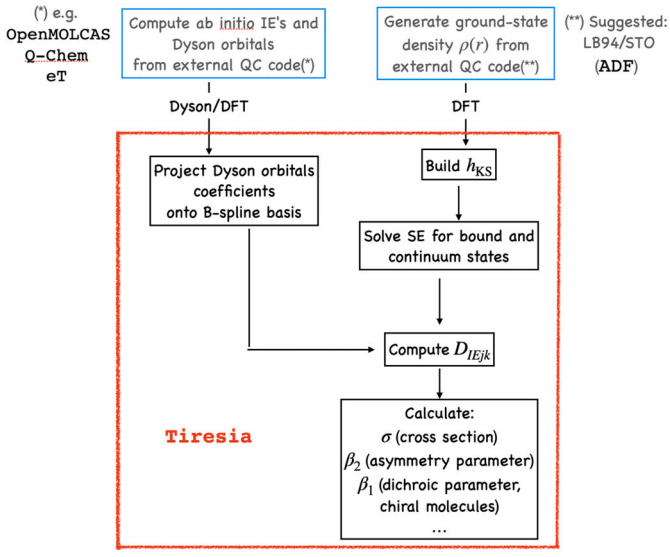

6. Photoionization observables

A program (`sdipole`) is available to print K-matrix and dipole matrix elements read from `fort.20` output from `Tiresia`, either in original form or transformed to incoming wave boundary condition, or also to (lm) partial waves, to be used for different analysis purposes. A second program, `sigma2`, is used to compute photoionization parameters for randomly oriented molecules, that is, partial cross section σ, asymmetry parameter β and chiral parameter β_1 for photoionization of chiral molecules [55]. For right and left Dyson orbitals, like those obtained from a coupled cluster calculation [17], one has to use `sigmalr11` instead of `sigma2`. A third program, `sigmanew`, can compute in addition cross sections in the molecular frame (MFPADS) from fixed in space molecules, following the formulation by Chandra [46,56], the

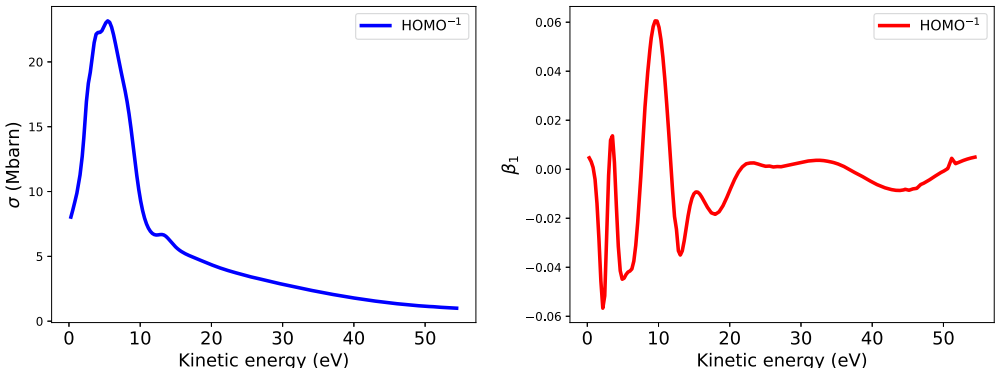

Fig. 4. Cross section (left) and dichroic parameter (right) relative to HOMO photoionization of Camphor.

so called polarized averaged MFPADS [57], and angular parameters following partial alignment from an initial photon absorption [58], to describe photoionization in pump-probe experiments. Further details are in the manual and in the examples provided. Details over more complex averages due to alignment/orientation characterized by a probability distribution of molecular axes are available from the authors.

A couple of results from the examples accompanying the code are briefly illustrated. Fig. 2 reports cross section σ and asymmetry parameter β for CO (over a shorter energy range), relative to the two outermost ionizations 5σ and 1π.

Both our standard LB94 DFT results (red curves) and results obtained employing the same potential, but HF density and initial orbitals (blue curves) are reported. Plenty of comparisons with experimental data are available [59,60], and show quite good agreement with the DFT results. Comparison with those from the same potential, but HF GTO densities and orbitals, show a fair general agreement, but significant differences in detail, especially on σ in the region close to the threshold, and some small spurious oscillations that are traced to the sensitivity of the density gradient employed in LB94 to inaccurate long-range behavior of the GTO representation. In general, however, the difference is comparable to the overall accuracy of the DFT approach.

An illustration of MFPADS relative to the 5σ ionization in CO, at electron kinetic energy KE = 0.2 au (photon energy is 19.8 eV, based on the 5σ eigenvalue) is presented in Fig. 3 for both parallel ($\beta = 0°$) and perpendicular ($\beta = 90°$) orientation of the electric field in the molecular frame. Although roughly following the electric field orientation, it shows a large anisotropy due to the interplay of different partial waves, which is generally also strongly energy dependent and is very specific of the initial orbital [6].

Finally, cross section σ and dichroic parameter β_1 are reported in Fig. 4 relative to the HOMO ionization of camphor. Of particular interest is the highly structured β_1 profile, which is one of the prominent probes of molecular chirality in the gas phase [6]. It can be compared to experimental results and previous calculations [34]. It illustrates the sensitivity of the low KE region to the specific potential choice. Since the β_1 parameter dies fast with increasing KE, the low energy region is however very relevant. In this case, we tried the VWN potential with a Coulomb tail, and obtained a reasonable description, improving on the previous LB94 calculations. It points out the need for further study to improve the many-particle description of photoionization close to the threshold, amenable to the treatment of complex molecules.

7. Conclusion

The `Tiresia` program has been presented, and its structure and capabilities illustrated. Its main purpose is the fast calculation of photoionization observables for complex molecules at the static DFT level. The structure of the LCAO B-spline basis is very accurate and complete, and can be used for a variety of additional purposes, including solution of linear operator equations, homogeneous and inhomogeneous with given boundary conditions, PT formulations, and wavepacket propagation by solution of the TDSE.

CRediT authorship contribution statement

All authors contributed equally.

Declaration of competing interest

The authors declare that they have no known competing financial interests or personal relationships that could have appeared to influence the work reported in this paper.

Data availability

Data will be made available on request.

Acknowledgement

It is a pleasure to acknowledge the long and productive collaboration with Fernando Martín and his group (Universidad Autónoma de Madrid, Spain) and Alejandro Saenz (Humboldt University of Berlin, Germany), where many ideas were discussed. Also, collaboration with Vitali Averbukh and Marco Ruberti (Imperial College London, UK); Torsha Moitra (UiT, The Arctic University of Norway), Bruno Tenorio (DTU, Technical University of Denmark), and Aurora Ponzi (University of Trieste and R. Bošković Institute, Zagreb, Croatia) in particular for their work interfacing Dyson orbitals to Tiresia; Nadja Doslic and her group (R. Bošković Institute, Zagreb, Croatia); David Ayuso and Olga Smirnova, (Max Planck Institute, Berlin, Germany). Computer time generously provided by CINECA for many of the results reported is gratefully acknowledged. SC acknowledges support from the Independent Research Fund Denmark, Grant No 7014-00258B, and the Research Council of Norway through FRINATEK project 275506 (Theolight). We also acknowledge the Marie Skłodowska-Curie European Training Network COSINE, Grant No. 765739. This publication is based upon work from COST Action AttoChem, CA18222, supported by COST (European Cooperation in Science and Technology). An STSM grant to Torsha Moitra (E-COST-GRANT-CA18222-36c84dc8) is also acknowledged.

Appendix A. Supplementary material

Supplementary material related to this article can be found online at https://doi.org/10.1016/j.cpc.2023.109038.

References

[1] P. Decleva, M. Stener, D. Toffoli, Continuum electronic states: the Tiresia code, Molecules 27 (6) (2022) 1–21, https://doi.org/10.3390/molecules27062026.
[2] T. Helgaker, P. Jørgensen, J. Olsen, Molecular Electronic-Structure Theory, John Wiley & Sons, Ltd, 2000.

[3] B.O. Roos, R. Lindh, P.A. Malmqvist, V. Veryazov, P.-O. Widmark, Multiconfigurational Quantum Chemistry, Wiley, Hoboken, 2016.

[4] J. Berkowitz, Atomic and Molecular Photoabsorption - Absolute Total Cross Sections, Academic Press, London, 2002.

[5] L. Young, K. Ueda, M. Gühr, P.H. Bucksbaum, M. Simon, S. Mukamel, N. Rohringer, K.C. Prince, C. Masciovecchio, M. Meyer, A. Rudenko, D. Rolles, C. Bostedt, M. Fuchs, D.A. Reis, R. Santra, H. Kapteyn, M. Murnane, H. Ibrahim, F. Légaré, M. Vrakking, M. Isinger, D. Kroon, M. Gisselbrecht, A. L'Huillier, H.J. Wörner, S.R. Leone, Roadmap of ultrafast x-ray atomic and molecular physics, J. Phys. B, At. Mol. Opt. Phys. 51 (3) (2018) 032003, https://doi.org/10.1088/1361-6455/aa9735.

[6] D. Dowek, P. Decleva, Trends in angle-resolved molecular photoelectron spectroscopy, Phys. Chem. Chem. Phys. 24 (2022) 24614–24654, https://doi.org/10.1039/D2CP02725A.

[7] R. Pazourek, S. Nagele, J. Burgdörfer, Attosecond chronoscopy of photoemission, Rev. Mod. Phys. 87 (2015) 765–802, https://doi.org/10.1103/RevModPhys.87.765.

[8] F.A. Gianturco, R.R. Lucchese, N. Sanna, Calculation of low-energy elastic cross sections for electron-CF_4 scattering, J. Chem. Phys. 100 (9) (1994) 6464–6471, https://doi.org/10.1063/1.467237.

[9] A.P.P. Natalense, R.R. Lucchese, Cross section and asymmetry parameter calculation for sulfur 1s photoionization of SF_6, J. Chem. Phys. 111 (12) (1999) 5344–5348, https://doi.org/10.1063/1.479794.

[10] Z. Mašín, J. Benda, J.D. Gorfinkiel, A.G. Harvey, J. Tennyson, UKRmol+: a suite for modelling electronic processes in molecules interacting with electrons, positrons and photons using the R-matrix method, Comput. Phys. Commun. 249 (2020) 107092, https://doi.org/10.1016/j.cpc.2019.107092.

[11] C. Marante, M. Klinker, I. Corral, J. González-Vázquez, L. Argenti, F. Martín, Hybrid-basis close-coupling interface to quantum chemistry packages for the treatment of ionization problems, J. Chem. Theory Comput. 13 (2) (2017) 499–514, https://doi.org/10.1021/acs.jctc.6b00907.

[12] F. Martín, J. González-Vázquez, I. Corral, J.V. Borràs, M. Klinker, L. Argenti, C. Marante, XCHEM - the ab initio solution for multichannel scattering problems, https://doi.org/10.21950/GHWTML, 2023.

[13] B.T. Pickup, On the theory of fast photoionization processes, Chem. Phys. 19 (2) (1977) 193–208, https://doi.org/10.1016/0301-0104(77)85131-8.

[14] L.S. Cederbaum, J. Schirmer, W. Domcke, W. von Niessen, Complete breakdown of the quasiparticle picture for inner valence electrons, J. Phys. B, At. Mol. Phys. 10 (15) (1977) L549–L553, https://doi.org/10.1088/0022-3700/10/15/001.

[15] R. Arneberg, J. Müller, R. Manne, Configuration interaction calculations of satellite structure in photoelectron spectra of H_2O, Chem. Phys. 64 (2) (1982) 249–258, https://doi.org/10.1016/0301-0104(82)87091-2.

[16] J.V. Ortiz, Dyson-orbital concepts for description of electrons in molecules, J. Chem. Phys. 153 (7) (2020) 070902, https://doi.org/10.1063/5.0016472.

[17] T. Moitra, A. Ponzi, H. Koch, S. Coriani, P. Decleva, Accurate description of photoionization dynamical parameters, J. Phys. Chem. Lett. 11 (13) (2020) 5330–5337, https://doi.org/10.1021/acs.jpclett.0c01337.

[18] C.M. Oana, A.I. Krylov, Dyson orbitals for ionization from the ground and electronically excited states within equation-of-motion coupled-cluster formalism: theory, implementation, and examples, J. Chem. Phys. 127 (23) (2007) 234106, https://doi.org/10.1063/1.2805393.

[19] B.N.C. Tenorio, A. Ponzi, S. Coriani, P. Decleva, Photoionization observables from multi-reference Dyson orbitals coupled to B-spline DFT and TD-DFT continuum, Molecules 27 (4) (2022) 1203, https://doi.org/10.3390/molecules27041203.

[20] T. Moitra, A.C. Paul, P. Decleva, H. Koch, S. Coriani, Multi-electron excitation contributions towards primary and satellite states in the photoelectron spectrum, Phys. Chem. Chem. Phys. 24 (2022) 8329–8343, https://doi.org/10.1039/D1CP04695K.

[21] P.V. Demekhin, A. Ehresmann, V.L. Sukhorukov, Single center method: a computational tool for ionization and electronic excitation studies of molecules, J. Chem. Phys. 134 (2) (2011) 024113, https://doi.org/10.1063/1.3526026.

[22] M. Stener, G. De Alti, P. Decleva, Convergence of the density functional one-centre expansion for the molecular continuum: N_2 and $(CH_3)_3N$, Theor. Chem. Acc. (Theor. Chim. Acta) 101 (1999) 247–256, https://doi.org/10.1007/s002140050437.

[23] D. Toffoli, M. Stener, G. Fronzoni, P. Decleva, Convergence of the multicenter B-spline DFT approach for the continuum, Chem. Phys. 276 (1) (2002) 25–43, https://doi.org/10.1016/S0301-0104(01)00549-3.

[24] H. Bachau, E. Cormier, P. Decleva, J.E. Hansen, F. Martín, Applications of B-splines in atomic and molecular physics, Rep. Prog. Phys. 64 (12) (2001) 1815–1943, https://doi.org/10.1088/0034-4885/64/12/205.

[25] P.G. Burke, R-Matrix Theory of Atomic Collisions: Application to Atomic, Molecular and Optical Processes, Springer, 2011.

[26] C. Froese Fischer, M. Idrees, Spline algorithms for continuum functions, Comput. Phys. 3 (3) (1989) 53–58, https://doi.org/10.1063/1.168325.

[27] M. Brosolo, P. Decleva, Variational approach to continuum orbitals in a spline basis: an application to H_2^+ photoionization, Chem. Phys. 159 (2) (1992) 185–196, https://doi.org/10.1016/0301-0104(92)80069-8.

[28] M. Brosolo, P. Decleva, A. Lisini, Continuum wavefunctions calculations with least-squares schemes in a B-splines basis, Comput. Phys. Commun. 71 (3) (1992) 207–214, https://doi.org/10.1016/0010-4655(92)90009-N.

[29] S.K. Semenov, N.A. Cherepkov, Generalization of the atomic RPA method for diatomic molecules: H_2 photoionization cross-section calculation, Chem. Phys. Lett. 291 (3) (1998) 375–380, https://doi.org/10.1016/S0009-2614(98)00573-9.

[30] Z.H. Levine, P. Soven, Time-dependent local-density theory of dielectric effects in small molecules, Phys. Rev. A 29 (1984) 625–635, https://doi.org/10.1103/PhysRevA.29.625.

[31] M. Stener, G. Fronzoni, P. Decleva, Time-dependent density-functional theory for molecular photoionization with noniterative algorithm and multicenter B-spline basis set: CS_2 and C_6H_6 case studies, J. Chem. Phys. 122 (23) (2005) 234301, https://doi.org/10.1063/1.1937367.

[32] C. Lee, W. Yang, R.G. Parr, Development of the Colle-Salvetti correlation-energy formula into a functional of the electron density, Phys. Rev. B 37 (1988) 785.

[33] J.C. Slater, Statistical Exchange-Correlation in the Self-Consistent Field, Advances in Quantum Chemistry, vol. 6, Academic Press, 1972, pp. 1–92.

[34] L. Nahon, L. Nag, G.A. Garcia, I. Myrgorodska, U. Meierhenrich, S. Beaulieu, V. Wanie, V. Blanchet, R. Géneaux, I. Powis, Determination of accurate electron chiral asymmetries in fenchone and camphor in the VUV range: sensitivity to isomerism and enantiomeric purity, Phys. Chem. Chem. Phys. 18 (2016) 12696–12706, https://doi.org/10.1039/C6CP01293K.

[35] S.H. Vosko, L. Wilk, M. Nusair, Accurate spin-dependent electron liquid correlation energies for local spin density calculations: a critical analysis, Can. J. Phys. 58 (8) (1980) 1200–1211, https://doi.org/10.1139/p80-159.

[36] R. van Leeuwen, E.J. Baerends, Exchange-correlation potential with correct asymptotic behavior, Phys. Rev. A 49 (1994) 2421–2431, https://doi.org/10.1103/PhysRevA.49.2421.

[37] M. Stener, S. Furlan, P. Decleva, Density functional calculations of photoionization with an exchange-correlation potential with the correct asymptotic behaviour, J. Phys. B, At. Mol. Opt. 33 (5) (2000) 1081–1102, https://doi.org/10.1088/0953-4075/33/5/321.

[38] G. te Velde, F.M. Bickelhaupt, E.J. Baerends, C. Fonseca Guerra, S.J.A. van Gisbergen, J.G. Snijders, T. Ziegler, Chemistry with ADF, J. Comput. Chem. 22 (9) (2001) 931–967, https://doi.org/10.1002/jcc.1056.

[39] E. Van Lenthe, E.J. Baerends, Optimized Slater-type basis sets for the elements 1-118, J. Comput. Chem. 24 (9) (2003) 1142–1156, https://doi.org/10.1002/jcc.10255.

[40] A. Ponzi, C. Angeli, R. Cimiraglia, S. Coriani, P. Decleva, Dynamical photoionization observables of the CS molecule: the role of electron correlation, J. Chem. Phys. 140 (20) (2014) 204304, https://doi.org/10.1063/1.4876495.

[41] G.L. Manni, I. Fdez. Galván, A. Alavi, F. Aleotti, F. Aquilante, J. Autschbach, D. Avagliano, A. Baiardi, J.J. Bao, S. Battaglia, L. Birnoschi, A. Blanco-González, S.I. Bokarev, R. Broer, R. Cacciari, P.B. Calio, R.K. Carlson, R. Carvalho Couto, L. Cerdán, L.F. Chibotaru, N.F. Chilton, J.R. Church, I. Conti, S. Coriani, J. Cuéllar-Zuquin, R.E. Daoud, N. Dattani, P. Decleva, C. de Graaf, M.G. Delcey, L.D. Vico, W. Dobrautz, S.S. Dong, R. Feng, N. Ferré, M. Filatov(Gulak), L. Gagliardi, M. Garavelli, L. González, Y. Guan, M. Guo, M.R. Hennefarth, M.R. Hermes, C.E. Hoyer, M. Huix-Rotllant, V.K. Jaiswal, A. Kaiser, D.S. Kaliakin, M. Khamesian, D.S. King, V. Kochetov, M. Krośnicki, A.A. Kumaar, E.D. Larsson, S. Lehtola, M.-B. Lepetit, H. Lischka, P. López Ríos, M. Lundberg, D. Ma, S. Mai, P. Marquetand, I.C.D. Merritt, F. Montorsi, M. Mörchen, A. Nenov, V.H.A. Nguyen, Y. Nishimoto, M.S. Oakley, M. Olivucci, M. Oppel, D. Padula, R. Pandharkar, Q.M. Phung, F. Plasser, G. Raggi, E. Rebolini, M. Reiher, I. Rivalta, D. Roca-Sanjuán, T. Romig, A.A. Safari, A. Sánchez-Mansilla, A.M. Sand, I. Schapiro, T.R. Scott, J. Segarra-Martí, F. Segatta, D.-C. Sergentu, P. Sharma, R. Shepard, Y. Shu, J.K. Staab, T.P. Straatsma, L.K. Sørensen, B.N.C. Tenorio, D.G. Truhlar, L. Ungur, M. Vacher, V. Veryazov, T.A. Voss, O. Weser, D. Wu, X. Yang, D. Yarkony, C. Zhou, J.P. Zobel, R. Lindh, The OpenMolcas Web: a community-driven approach to advancing computational chemistry, J. Chem. Theory Comput. (2023), https://doi.org/10.1021/acs.jctc.3c00182.

[42] E. Epifanovsky, A.T.B. Gilbert, X. Feng, J. Lee, Y. Mao, N. Mardirossian, P. Pokhilko, A.F. White, M.P. Coons, A.L. Dempwolff, Z. Gan, D. Hait, P.R. Horn, L.D. Jacobson, I. Kaliman, J. Kussmann, A.W. Lange, K.U. Lao, D.S. Levine, J. Liu, S.C. McKenzie, A.F. Morrison, K.D. Nanda, F. Plasser, D.R. Rehn, M.L. Vidal, Z.-Q. You, Y. Zhu, B. Alam, B.J. Albrecht, A. Aldossary, E. Alguire, J.H. Andersen, V. Athavale, D. Barton, K. Begam, A. Behn, N. Bellonzi, Y.A. Bernard, E.J. Berquist, H.G.A. Burton, A. Carreras, K. Carter-Fenk, R. Chakraborty, A.D. Chien, K.D. Closser, V. Cofer-Shabica, S. Dasgupta, M. de Wergifosse, J. Deng, M. Diedenhofen, H. Do, S. Ehlert, P.-T. Fang, S. Fatehi, Q. Feng, T. Friedhoff, J. Gayvert, Q. Ge, G. Gidofalvi, M. Goldey, J. Gomes, C.E. González-Espinoza, S. Gulania, A.O. Gunina, M.W.D. Hanson-Heine, P.H.P. Harbach, A. Hauser, M.F. Herbst, M. Hernández Vera, M. Hodecker, Z.C. Holden, S. Houck, X. Huang, K. Hui, B.C. Huynh, M. Ivanov, Á. Jász, H. Ji, H. Jiang, B. Kaduk, S. Kähler, K. Khistyaev, J. Kim, G. Kis, P. Klunzinger, Z. Koczor-Benda, J.H. Koh, D. Kosenkov, L. Koulias, T. Kowalczyk, C.M. Krauter, K. Kue, A. Kunitsa, T. Kus, I. Ladjánszki, A. Landau, K.V. Lawler, D. Lefrancois, S. Lehtola, R.R. Li, Y.-P. Li, J. Liang, M. Liebenthal, H.-H. Lin, Y.-S. Lin, F. Liu, K.-Y. Liu, M. Loipersberger, A. Luenser, A. Manjanath, P. Manohar, E. Mansoor, S.F. Manzer, S.-P. Mao, A.V. Marenich, T. Markovich, S. Mason, S.A. Maurer, P.F. McLaughlin, M.F.S.J. Menger, J.-M. Mewes, S.A. Mewes, P. Morgante, J.W. Mullinax, K.J. Oosterbaan, G. Paran, A.C. Paul, S.K. Paul, F. Pavošević, Z. Pei, S. Prager, E.I. Proynov, Á. Rák, E. Ramos-Cordoba, B. Rana, A.E. Rask, A. Rettig, R.M. Richard, F. Rob, E. Rossomme, T. Scheele, M. Scheurer, M. Schneider, N. Sergueev, S.M. Sharada, W. Skomorowski, D.W. Small, C.J. Stein, Y.-C. Su, E.J. Sundstrom, Z. Tao, J. Thirman, G.J. Tornai, T. Tsuchimochi, N.M. Tubman, S.P. Veccham, O. Vydrov, J. Wenzel, J. Witte, A. Yamada, K. Yao, S. Yeganeh, S.R. Yost, A. Zech, I.Y. Zhang, X. Zhang, Y. Zhang, D. Zuev, A. Aspuru-Guzik, A.T. Bell, N.A. Besley, K.B. Bravaya, B.R. Brooks, D. Casanova, J.-D. Chai, S.

Coriani, C.J. Cramer, G. Cserey, A.E. DePrince, R.A. DiStasio, A. Dreuw, B.D. Dunietz, T.R. Furlani, W.A. Goddard, S. Hammes-Schiffer, T. Head-Gordon, W.J. Hehre, C.-P. Hsu, T.-C. Jagau, Y. Jung, A. Klamt, J. Kong, D.S. Lambrecht, W. Liang, N.J. Mayhall, C.W. McCurdy, J.B. Neaton, C. Ochsenfeld, J.A. Parkhill, R. Peverati, V.A. Rassolov, Y. Shao, L.V. Slipchenko, T. Stauch, R.P. Steele, J.E. Subotnik, A.J.W. Thom, A. Tkatchenko, D.G. Truhlar, T. Van Voorhis, T.A. Wesolowski, K.B. Whaley, H.L. Woodcock, P.M. Zimmerman, S. Faraji, P.M.W. Gill, M. Head-Gordon, J.M. Herbert, A.I. Krylov, Software for the frontiers of quantum chemistry: an overview of developments in the Q-Chem 5 package, J. Chem. Phys. 155 (8) (2021) 084801, https://doi.org/10.1063/5.0055522.

[43] S.D. Folkestad, E.F. Kjønstad, R.H. Myhre, J.H. Andersen, A. Balbi, S. Coriani, T. Giovannini, L. Goletto, T.S. Haugland, A. Hutcheson, I.-M. Høyvik, T. Moitra, A.C. Paul, M. Scavino, A.S. Skeidsvoll, Å.H. Tveten, H. Koch, e^T 1.0: an open source electronic structure program with emphasis on coupled cluster and multilevel methods, J. Chem. Phys. 152 (18) (2020) 184103, https://doi.org/10.1063/5.0004713.

[44] C. de Boor, A Practical Guide to Splines, Springer, New York, 1978.

[45] P.G. Burke, N. Chandra, F.A. Gianturco, Electron-molecule interactions. IV. Scattering by polyatomic molecules, J. Phys. B, At. Mol. Phys. 5 (12) (1972) 2212, https://doi.org/10.1088/0022-3700/5/12/015.

[46] N. Chandra, Photoelectron spectroscopic studies of polyatomic molecules. I. Theory, J. Phys. B, At. Mol. Phys. 20 (14) (1987) 3405, https://doi.org/10.1088/0022-3700/20/14/013.

[47] N. Chandra, Photoelectron spectroscopic studies of polyatomic molecules. II. Ionisation in the a_1 orbital of a T_d molecule, J. Phys. B, At. Mol. Phys. 20 (14) (1987) 3417, https://doi.org/10.1088/0022-3700/20/14/014.

[48] E. Kukk, T.D. Thomas, K. Ueda, D. Céolin, S. Granroth, K. Kooser, O. Travnikova, D. Iablonsky, P. Decleva, D. Ayuso, R. Püttner, H. Levola, G. Goldsztejn, T. Marchenko, M.N. Piancastelli, M. Simon, Photoelectron recoil in CO in the x-ray region up to 7 keV, Phys. Rev. A 95 (2017) 042509, https://doi.org/10.1103/PhysRevA.95.042509.

[49] L.S. Blackford, J. Choi, A. Cleary, E. D'Azeuedo, J. Demmel, I. Dhillon, S. Hammarling, G. Henry, A. Petitet, K. Stanley, D. Walker, R.C. Whaley, J.J. Dongarra, ScaLAPACK User's Guide, Society for Industrial and Applied Mathematics, USA, 1997.

[50] C.F. Fischer, M. Idrees, Spline methods for resonances in photoionisation cross sections, J. Phys. B, At. Mol. Opt. Phys. 23 (4) (1990) 679–691, https://doi.org/10.1088/0953-4075/23/4/002.

[51] M. Brosolo, P. Decleva, A. Lisini, LCAO expansion in a spline basis for accurate variational determination of continuum wavefunctions. Applications to H_2^+ and HeH^{2+}, Chem. Phys. 181 (1) (1994) 85–95, https://doi.org/10.1016/0301-0104(94)85017-8.

[52] S. Petretti, Y.V. Vanne, A. Saenz, A. Castro, P. Decleva, Alignment-dependent ionization of N_2, O_2, and CO_2 in intense laser fields, Phys. Rev. Lett. 104 (2010) 223001, https://doi.org/10.1103/PhysRevLett.104.223001.

[53] E. Plésiat, M. Lara-Astiaso, P. Decleva, A. Palacios, F. Martín, Real-time imaging of ultrafast charge dynamics in tetrafluoromethane from attosecond pump-probe photoelectron spectroscopy, Chem. Eur. J. 24 (46) (2018) 12061–12070, https://doi.org/10.1002/chem.201802788.

[54] S. Nandi, E. Plésiat, S. Zhong, A. Palacios, D. Busto, M. Isinger, L. Neoričić, C.L. Arnold, R.J. Squibb, R. Feifel, P. Decleva, A. L'Huillier, F. Martín, M. Gisselbrecht, Attosecond timing of electron emission from a molecular shape resonance, Sci. Adv. 6 (31) (2020) eaba7762, https://doi.org/10.1126/sciadv.aba7762.

[55] S. Stranges, S. Turchini, M. Alagia, G. Alberti, G. Contini, P. Decleva, G. Fronzoni, M. Stener, N. Zema, T. Prosperi, Valence photoionization dynamics in circular dichroism of chiral free molecules: the methyl-oxirane, J. Chem. Phys. 122 (24) (2005) 244303, https://doi.org/10.1063/1.1940632.

[56] M. Stener, Photoionization of oriented molecules: a time dependent density functional approach, Chem. Phys. Lett. 356 (1) (2002) 153–160, https://doi.org/10.1016/S0009-2614(02)00382-2.

[57] E. Plésiat, P. Decleva, F. Martín, Relationship between polarization-averaged molecular-frame photoelectron angular distributions and geometry, Phys. Rev. A 88 (2013) 063409, https://doi.org/10.1103/PhysRevA.88.063409.

[58] A. Humeniuk, M. Wohlgemuth, T. Suzuki, R. Mitrić, Time-resolved photoelectron imaging spectra from non-adiabatic molecular dynamics simulations, J. Chem. Phys. 139 (13) (2013) 134104, https://doi.org/10.1063/1.4820238.

[59] M. Stener, P. Decleva, I. Cacelli, R. Moccia, R. Montuoro, Response function study of CO photoionization: ab initio SCF and density functional results, Chem. Phys. 272 (1) (2001) 15–25, https://doi.org/10.1016/S0301-0104(01)00458-X.

[60] E. Plésiat, P. Decleva, F. Martín, Vibrational branching ratios in the photoelectron spectra of N_2 and CO: interference and diffraction effects, Phys. Chem. Chem. Phys. 14 (2012) 10853–10871, https://doi.org/10.1039/C2CP40693D.